Nanoscale

Accepted Manuscript

This article can be cited before page numbers have been issued, to do this please use: X. He, Z. Wang, Z. Jin, L. Qiao, H. Zhang and N. Chen, *Nanoscale*, 2025, DOI: 10.1039/D5NR01104C.

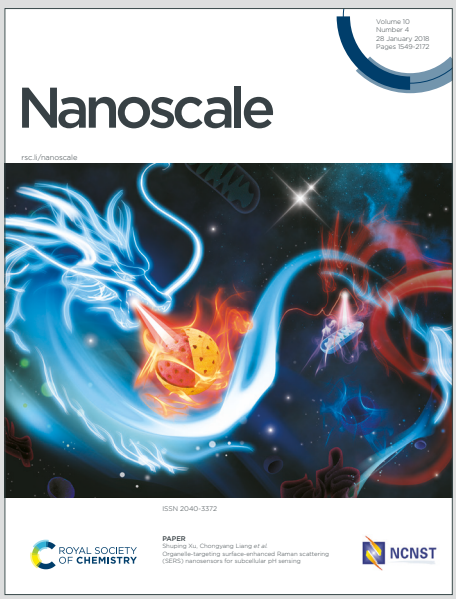

ROYAL SOCIETY OF CHEMISTRY

rsc.li/nanoscale

View Article Online
DOI: 10.1039/D5NR01104C

ARTICLE

2D Carbon's Dual Pioneers: Graphene Oxide and Graphdiyne Guiding Solar Evaporation through Three-Dimensional Mastery

Received 00th January 20xx,
Accepted 00th January 20xx

DOI: 10.1039/x0xx00000x

Xiaojun He,[a,b,c] Zhenglin Wang,[a,b,c] Zifeng Jin,[a,b,c] Lanmin Qiao,[a,b,c] Hui Zhang,[a,b,c] Nan Chen[a,b,c,*]

Carbon-based two-dimensional (2D) materials, graphene oxide (GO) and graphdiyne (GDY), emerge as dual pioneers in Solar-powered water purification technology by mastering three-dimensional (3D) optimization: broadband photon harvesting, localized thermal management, and controllable water transport. This review dissects how their unique hybridization modes—GO's sp^2/sp^3 heterostructure and GDY's sp/sp^2-conjugated lattice—synergize to govern these tripartite mechanisms. First, orbital engineering in GO extends π-π* transitions for a high solar absorption, while GDY's Dirac-cone bandgap enables ultrafast hot-carrier generation. Second, thermal confinement is achieved through GO's anisotropic heat dissipation and GDY's proton-relay networks, minimizing parasitic losses. Third, the electrostatic force elimination effect of GO, coupled with GDY's nanometer-scale channel regulation, enables efficient ion separation and screening. Critically, we demonstrate how these three dimensions—light, heat, and mass—are interlocked: GO's hydrophilicity accelerates evaporation kinetics, while GDY's structural flexibility tailors water pathways. Challenges such as GO's oxidation instability and GDY's scalable synthesis are addressed, with future directions advocating machine learning-driven hybridization control and modular evaporator designs. This work redefines "3D mastery" as a paradigm integrating spectral, thermal, and fluidic optimization, offering a roadmap for next-generation solar water-energy systems.

1. Introduction

The contemporary global landscape is characterized by accelerating industrialization and urbanization, which have driven an unprecedented demand for improved energy efficiency across various sectors. Paradoxically, freshwater scarcity remains a growing challenge, fundamentally limiting global sustainable development [1]. Given the severe scarcity of water resources, researchers have explored various artificial water purification methods, such as multi-stage flash evaporation, low-temperature multi-effect evaporation, and reverse osmosis. However, these methods still face certain limitations in terms of energy consumption, cost, and efficiency [2]. The hydrological cycle (Figure 1a) highlights the critical role of evaporation in freshwater generation, which can be amplified by solar-driven interfacial evaporation technologies [3]. Among these, the evaporation phase has been identified as containing the highest concentration potential for harvestable freshwater resources, presenting a vital opportunity for technological intervention. Breakthroughs in material science have demonstrated that nanostructured photothermal-responsive materials exhibit remarkable ability to selectively absorb solar radiation and convert it into localized thermal energy, thereby significantly accelerating evaporation dynamics.

This scientific breakthrough has catalyzed the emergence of interface solar-driven evaporation (ISDE) technology, representing a paradigm shift that not only achieves outstanding solar energy conversion efficiency but also enables sustainable and decentralized freshwater production through environmentally friendly processes[4, 5]. As shown in Figure 1b, the evolution of photothermal evaporation technology has gone through three distinct development phases. The first phase (2008-2015) relied on substrate-based thermal conduction systems, where submerged heating elements transferred heat via aqueous media. However, due to multi-wavelength light scattering and absorption within the water layer, this configuration led to significant energy losses (58-63% reduction in irradiance), resulting in solar-to-steam conversion efficiency of only 12-18%. Subsequent technological iterations (2016-2019) introduced dispersed photothermal nanofluids within bulk liquid matrices, enhancing light absorption through volumetric heating effects. However, sustained thermal convection losses and inefficient energy localization kept the actual efficiency below 35%. The current state-of-the-art paradigm (2020-present) incorporates precisely designed interface evaporation architectures, synergizing plasma absorbers with graded cellulose-based substrates. Through advanced thermal management strategies and biomimetic structural optimization, these systems exhibit groundbreaking efficiencies of 85-92% while minimizing parasitic heat loss through radiation cooling mechanisms [6].

[a] Key Laboratory of Cluster Science, Ministry of Education of China, Key Laboratory of Photoelectronic/Electrophotonic Conversion Materials, School of Chemistry and Chemical Engineering, Beijing Institute of Technology, No. 5, South Street, zhongguancun, Haidian District, Beijing, China 100081，E-mail: gabechain@bit.edu.cn
[b] Yangtze Delta Region Academy, Beijing Institute of Technology, No. 1940, Dongfang North Road, Youchegang Town, Xiuzhou District, Jiaxing, Zhejiang, China 314000.
[c] Tangshan Research Institute, Beijing Institute of Technology, No. 57, Jianshe South Road, Lubei District, Tangshan, Hebei, China 063000.

The photothermal conversion process is a cornerstone of the photothermal-based energy harvesting technologies, such as the ISDE technology. This process is underpinned by three principal energy transduction mechanisms, each of which has been rigorously studied and characterized at the molecular and nanoscale levels. The first mechanism involves the phenomenon of surface plasmon resonance (SPR), which occurs when the frequency of incident photons matches the collective oscillation frequency of conduction electrons in noble metal nanostructures, such as Au or Ag. The matching between the frequency of the incident light and the oscillation frequency of the delocalized electrons in the metal triggers the collective excitation of the electrons and the subsequent generation of thermal electrons. The excited thermal electrons oscillate coherently with the incident electromagnetic field and generate heat through the Joule mechanism (Figure 1c) [7]. Hot carriers rapidly redistribute their energy through the electron-electron scattering process, thereby heating the plasma element itself.

Figure 1. A brief theoretical overview of photothermal water evaporation. (a) Schematic diagram of the water cycle. (b) Development stages of photothermal water evaporation. (c) Plasmonic heating. (d) Electron - hole generation and relaxation. (e) Thermal vibration of molecules.

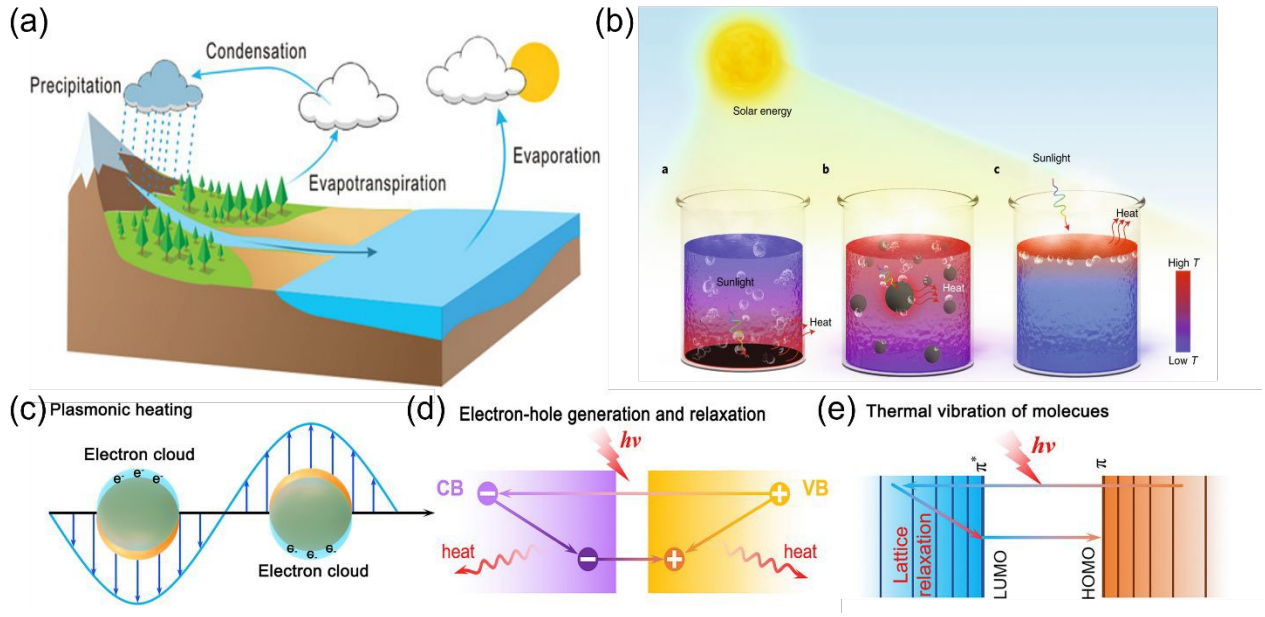

The second energy conversion pathway operates in narrow-bandgap semiconductors, such as $Ti_3C_2T_x$ MXenes or copper sulfide (CuS) nanocrystals. In these materials, supra-bandgap photon absorption leads to the excitation of electrons from the valence band to the conduction band, forming highly energetic electron-hole pairs. These non-equilibrium charge carriers undergo rapid thermalization, typically on timescales of less than 100 fs, via carrier-carrier scattering processes. During this ultrafast relaxation, excess kinetic energy is dissipated as vibrational energy through phonon interactions, and the charge carriers eventually relax towards the band edges. This rapid and efficient energy conversion mechanism enables the transformation of broad-spectrum solar irradiation into usable thermal energy, with the controlled Auger recombination process—where energy or momentum is transferred to another electron or hole through collisions during the recombination of electrons and holes in semiconductors, causing transitions of the involved particles—serving as a key mechanism for energy dissipation and thermal output (Figure 1d) [7].

The third mechanism exploits the molecular vibrational modes present in conjugated organic polymers, such as polypyrrole and PEDOT:PSS. Under visible-light irradiation, π-π* electronic transitions are excited, creating transient excitons. These photo-excited states rapidly decay through non-radiative relaxation pathways, during which vibrational energy is transferred to adjacent molecular chains via Förster resonance energy transfer (FRET), a non-radiative process in which energy is transferred from the excited state of the donor molecule to the acceptor molecule through dipole-dipole interactions [8]. The energy transferred in this manner accumulates and is eventually dissipated as macroscopic heating via phonon-phonon coupling in the crystalline domains of the polymer material. Notably, the thermal conductivity of these materials can be tuned by the functionalization of side chains, offering a flexible approach for optimizing thermal output in organic polymer-based photothermal devices (Figure 1e) [7]. Together, these three distinct yet complementary photothermal conversion mechanisms offer a versatile and highly efficient foundation for solar-driven energy conversion technologies. Through the precise modulation of material properties, such as nanostructure morphology, bandgap, and molecular functionality, it is possible to optimize the conversion of photon energy into thermal energy, making these processes ideal candidates for a range of applications in renewable energy harvesting and environmental management.

In the field of photothermal materials research, these systems can generally be classified into four categories: organic polymer materials, metal nanomaterials, inorganic

View Article Online
DOI: 10.1039/D5NR01104C

semiconductors, and carbon-based materials. Organic polymers are characterized by unique optical properties, structural diversity, tunable surface morphology, and controllable biodegradability, making them highly sustainable from an environmental perspective [9-11]. However, these materials tend to exhibit relatively low photothermal conversion efficiency and may undergo photodegradation under prolonged solar exposure. Metal nanoparticles, owing to localized surface plasmon resonance effects, serve as efficient solar energy converters. However, the practical implementation of metal-based systems faces numerous challenges, including complex synthesis protocols, environmental pollution risks, increased production costs, and suboptimal photothermal performance. Additionally, structural modifications are often required to adjust their absorption bandwidth [12, 13]. Furthermore, metal structures exhibit limited stability in acidic or alkaline environments, leading to structural degradation and shortened service life. Inorganic semiconductors are known for their compositional diversity, economic feasibility, excellent optical stability, and customizable morphology. The optical absorption properties of semiconductors show wavelength-dependent behavior, particularly near their bandgap energy. Upon light exposure, semiconductor materials generate electron-hole pairs, and their energy typically corresponds to the bandgap. These excited electrons ultimately relax to lower energy states through radiative photon emission or non-radiative phonon-mediated thermal dissipation [14]. However, achieving high conversion efficiency often requires strong illumination [15, 16].

Carbon-based materials, with their tunable bandgap structures and porous nature, exhibit broad solar spectrum absorption and excellent photothermal conversion efficiency. The unique hybridization of the s and p orbitals in carbon-based materials imparts exceptional thermal conductivity and remarkable physicochemical stability. Notably, 2D carbon derivatives such as GO and GDY, with their unique orbital hybridization, offer: (1) the ability for functional group modifications needed for designing composite photothermal systems, and (2) intrinsic structural robustness against environmental degradation. Additionally, these materials allow for micro/nano-structural engineering through various fabrication methods, facilitating the development of 3D devices suitable for diverse operating conditions [17]. The unparalleled structural properties of carbon-based systems establish their indispensable role in interface solar evaporation technologies, providing dual advantages: multifunctional integration for novel material development and design flexibility for customized evaporator configurations.

2. Structural Analysis and Applications of GO & GDY

The carbon-based materials primarily composed of single bonds (such as C-C, C-H, C-O) exhibit a significant energy gap (σ-σ* transition), corresponding to wavelengths below 350 nm in the solar spectrum. However, the σ→σ* transition induced under solar irradiation is thermodynamically challenging. In contrast, π bonds have a lower electron binding strength, which facilitates the π→π* excitation, reducing the required energy input [18, 19]. The extended π-conjugated system induces a redshift in the absorption spectrum, where an increase in the number of π bonds narrows the energy gap between the Highest Occupied Molecular Orbital (HOMO) and the Lowest Unoccupied Molecular Orbital (LUMO). In typical 2D carbon materials including GO and GDY, the extensive π-conjugated network enables wide-band solar absorption across nearly all wavelengths. The cumulative π-π* transitions give carbon materials their distinctive black appearance. As shown in Figure 1c, the photothermal mechanism involves electron excitation from the HOMO state to the LUMO state under resonant photon energy, followed by electron-phonon coupling relaxation, transferring energy to lattice vibrations, which then leads to a macroscopic temperature increase [20].

2.1. GO Structure and Applications.

Monolayer graphene, widely regarded as the quintessential 2D crystal, represents an ideal material in various fields due to its unique electronic, mechanical, and optical properties [21]. However, for practical applications in photothermal conversion, particularly in solar energy harvesting and desalination, graphene requires further functional modifications to enhance its performance and adaptability. One of the most promising derivatives of graphene for such applications is oxygen-rich GO, which stands out as a key 2D carbon material due to its tunable hydrophilicity and compatibility with a variety of composites (Figure 2a) [22]. The introduction of oxygen-containing functional groups, such as epoxides, hydroxyls, and carboxyls, into the graphene structure significantly enhances interfacial interactions, primarily through hydrogen bonding, thereby improving the material's wettability and its ability to absorb solar radiation efficiently. Both GO and its reduced form, reduced graphene oxide (rGO), retain these oxygenated functional groups, which play a crucial role in mediating the interactions between GO and water molecules, thus facilitating photothermal conversion. While mapping the precise distribution of oxygen groups on the GO surface remains a complex challenge, it is generally observed that rGO predominantly retains oxygen species located at the edges of the graphene sheets. These edge-functionalized oxygen groups are crucial in maintaining the material's functional properties, even after reduction [23, 24]. Furthermore, the supramolecular interactions that occur within the basal planes of GO/rGO contribute to the minimization of structural defects during composite material fabrication. This helps preserve the intrinsic photothermal properties, which are vital for applications requiring sustained thermal stability under light irradiation.

GO exhibits a distinctive dual hybridization of sp^2 and sp^3 carbon atoms, forming a mixed bonding structure. The sp^2 domains of GO contribute to broad light absorption across the visible to near-infrared (NIR) spectrum, making it highly suitable for photothermal energy harvesting. On the other hand, the sp^3-bonded oxygen groups (hydroxyl and carboxyl) significantly enhance GO's hydrophilicity by facilitating hydrogen bonding with water molecules, which in turn supports the material's use

in water-related applications such as solar desalination (Figure 2b) [25]. This dual-functional structure, combining the high conductivity and absorption capabilities of the sp² domains with the hydrophilic nature of the oxygenated groups, underpins the prominence of GO-based materials in solar-driven water

View Article Online
DOI: 10.1039/D5NR01104C

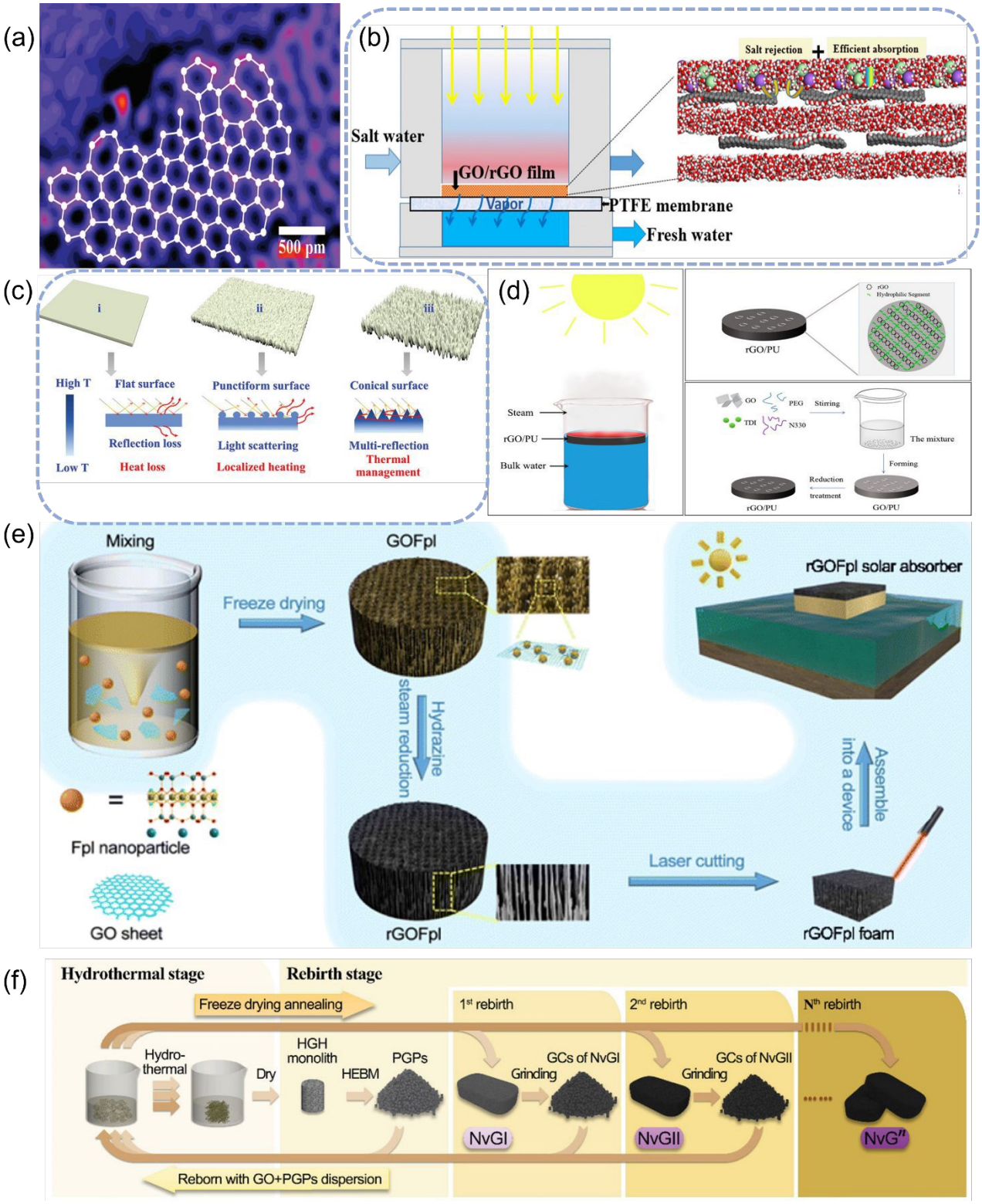

Figure 2. Schematic diagram of GO structure and applications. (a) Carbon atom configuration in GO. (b) A typical photothermal evaporation system based on GO. (c) 2D nanoscale water channels in the GO membrane. (d) Wood@GO bilayer structure. (e) Graphene-based foam (rGOFpl foam) containing high-polarity components is used for evaporator. (f) Nirvana graphene (NvG) obtained through repeated repetitive rebirth strategy.

View Article Online
DOI: 10.1039/D5NR01104C

evaporation and desalination processes. Several studies have leveraged these unique properties of GO to develop advanced photothermal systems. For example, Qiu et al. reported a new strategy for manipulating the surface morphology of GO through electrostatic assembly and in-situ polymerization of aniline. The GO surface is completely hybridized with polyaniline (PANI) nano cone arrays, exhibiting a highly foldable periodic structure that significantly increases its ability to absorb sunlight (Figure 2c) [26]. This configuration maximizes the material's efficiency in capturing solar energy and transferring it to the nanoscale water channels, thereby improving the overall water evaporation rate. In a similar vein, Liu et al. introduced a bilayer wood@GO evaporator that utilizes GO's broad light absorption spectrum for rapid interfacial heating (Figure 2d) [17]. This design enhances heat transfer efficiency and accelerates the evaporation process. Furthermore, Chen et al. designed a rGOFpl foam as a solar absorber featuring surface-enriched high-polarity units (Figure 2e). Experimental investigations coupled with theoretical simulations revealed that charge transfer induced by high-polarity components (e.g., MgF_2) at solid-liquid interfaces modifies the charge distribution of adjacent water molecules, promoting the formation of intermediate water layers with weakened intermolecular hydrogen bonds that facilitate evaporation[27]. Notably, GO demonstrates inherent advantages in alternative seawater desalination approaches such as capacitive deionization (CDI), as illustrated in Figure 2f. Qu group developed a 3D GO (3DG) material through a nirvana-like regeneration strategy, where each regeneration cycle progressively enhances material properties. The reborn 3DG, termed NvG, exhibits remarkable improvements over conventional 3DG, including 3.36-fold higher density, increased porosity, 1.41-fold enhanced conductivity, 32.4-fold greater mechanical strength, and ultrafast permeation behavior. These superior characteristics endow NvG with exceptional CDI performance, achieving a volumetric capacity of 220 F cm^{-3} at 1 A cm^{-3} and maximum salt adsorption capacity of 8.02-9.2 mg cm^{-3} (8.9-10.2 times enhancement). Remarkably, the energy consumption for equivalent salt adsorption is reduced to less than a quarter of that required by 3DG [28]. These advances collectively demonstrate that structural hybridization (sp^2/sp^3 domains), interfacial engineering (e.g., hydrogen bonding and charge transfer), and topology optimization (e.g., 3D porous networks) synergistically enhance GO/rGO as thermally robust photothermal platforms. Such multifunctional designs not only address energy-water nexus challenges in solar desalination and wastewater remediation but also open avenues for scalable solar-to-thermal energy conversion systems

2.2. GDY Structure and Applications

GDY, a novel carbon allotrope featuring sp/sp^2 hybridized networks [29, 30], was first successfully synthesized in 2010 by utilizing hexaethynylbenzene (HEB) precursors on flat Cu foil [31]. As depicted in Figures 3a and 3b, GDY's structure consists of hexagonal benzene rings that are interconnected by six –C≡C–C≡C– bonds, creating a single-atom-thick, 2D planar network [32]. The hybridization of carbon atoms within GDY primarily involves sp and sp^2 orbital configurations, leading to a distinctive atomic arrangement that imparts a range of exceptional physical and chemical properties. Specifically, the bond lengths of $C(sp^2)$–$C(sp^2)$ (between adjacent triple bonds), aromatic C(sp)–C(sp), C(sp)–$C(sp^2)$, and triple bonds in GDY are calculated to be 1.33 Å, 1.41 Å, 1.40 Å, and 1.24 Å, respectively. These values provide critical insights into the bonding and structural stability of GDY. Compared to graphene, GDY exhibits greater structural flexibility, enhanced chemical reactivity, and remarkable adaptability to various external stimuli [33]. This structural flexibility opens up new avenues for material modifications or defect engineering, which can significantly tailor GDY's properties, a key feature for optimizing GDY-based devices.

The unique atomic distribution and hybridization in GDY confer its exceptional characteristics, including diverse chemical bonding types, extended conjugation, a highly delocalized π-system, intrinsic nanoporosity, and high charge carrier mobility, all of which contribute to its superior electronic conductivity and mechanical stability. The sp-hybridized acetylene bonds in GDY are particularly noteworthy as they provide a distinct electronic structure that allows GDY to absorb a broader range of light, spanning from ultraviolet to visible wavelengths. This wide spectral absorption enhances its photothermal conversion efficiency, thereby maximizing its utilization of solar energy. The electronic structure of GDY is a key factor determining its material properties. Notably, GDY possesses Dirac cones and exhibits a direct bandgap, which renders it an excellent candidate for semiconductor and optoelectronic applications [34]. The theoretical direct bandgap of GDY is calculated to be 1.10 eV [32], which is close to the quasi-particle bandgap of silicon. However, due to the existence of a direct bandgap (which is quite advantageous for semiconductors and optoelectronic devices), GDY may have superior characteristics than silicon [35]. Nevertheless, this bandgap can be effectively tuned through several strategies, including the construction of nanoribbons [36, 37], the application of external strain [38], chemical functionalization [39, 40], and the use of electric fields [41]. These strategies allow for the precise modulation of GDY's electronic properties, further enhancing its potential for a wide range of advanced technological applications.

Later studies successfully achieved the fabrication of ultrathin GDY membranes with a remarkable thickness of approximately 0.6 nm, utilizing atmospheric-pressure chemical vapor deposition (APCVD) methods [42]. The vapor-liquid-solid (VLS) technique has also been explored, enabling the production of smooth GDY films with thicknesses ranging from 22 nm to 540 nm, thus offering a scalable approach for fabricating GDY materials with tunable thicknesses and properties [43]. However, the synthesis of highly crystalline monolayer or few-layer GDY has remained challenging, primarily due to the instability of HEB monomers during the coupling process. To overcome these challenges, Zhang et al. introduced a microwave-assisted synthesis method that stabilizes HEB monomers via a temperature gradient, enabling few-layer GDY production with sub-2 nm thickness. The

View Article Online
DOI: 10.1039/D5NR01104C

produced GDY exhibited p-type semiconducting behavior, with a remarkable field-effect mobility of 50.1 $cm^2 V^{-1} \cdot s^{-1}$

Figure 3. Structural and functional analysis of GDY. (a) Geometric and electronic band structures of monolayer GDY. (b) Top-view optimized configurations of bilayer GDY. (c) Microwave-synthesized GDY film. (d) Mo^0/GDY single-atom catalyst for efficient NH_3/H_2 production. (e) Synthesis strategy for OsO_x-QD/GDY hybrids. (f) GDY/CuO high-efficiency photothermal evaporator.

demonstrating the potential of this method in producing high-quality GDY films (Figure 3c) [44]. This advancement marked a significant step toward overcoming the synthesis challenges and expanding the practical applications of GDY in various fields. The unique structural characteristics of GDY, including its extended conjugated π-system and two-dimensional nature, provide it with a range of extraordinary properties that make it a promising candidate for numerous applications. For instance, Li et al. developed a Mo^0-loaded GDY single-atom catalyst that exhibited high catalytic efficiency for selective ammonia and hydrogen production, highlighting the dual-function catalytic potential of GDY-based materials (Figure 3d) [45]. Additionally, Du et al. grew OsO_x quantum dots on a 3D flexible GDY substrate for photoelectrocatalytic applications, significantly enhancing the hydrogen evolution reaction (HER) activity under illumination, thereby further emphasizing the versatility of GDY in catalysis (Figure 3e) [46]. Furthermore, Zhang et al. designed a GDY/CuO nanowire foam structure, enabling effective photothermal conversion of the solar spectrum and demonstrating exceptional water evaporation performance, thus validating the applicability of GDY across ISDE field (Figure 3f) [47].

Carbon-based 2D materials, such as GO and GDY, exhibit extraordinary properties due to their diverse hybridization modes, which make them suitable for a wide range of multidisciplinary applications. In the context of photothermal interfacial evaporation, where material properties and structural requirements vary, the tunable 3D morphology of GO and the compatibility of GDY with composite materials—while retaining their intrinsic properties—make these materials highly versatile and ideal for advanced applications in this field. Their unique structural features and functionalization possibilities offer novel perspectives for designing next-generation photothermal systems and integrating multifunctional resources, opening up new avenues for the development of advanced materials and devices across various technological domains.

3. Design Optimization Strategies for Photothermal Evaporation

ISDE systems, particularly those based on interfacial solar evaporators, rely on the integration of two synergistic

components: material design and optimization of transport behavior. The material design aspect primarily governs the energy conversion processes during the evaporation process. Specifically, in photothermal evaporation, the photon energy harvested from sunlight is absorbed by photothermal materials and subsequently converted into thermal energy. This thermal energy is transferred to the aqueous media, promoting the phase transition of water molecules from liquid to vapor. Within this context, two key factors are of paramount importance: (1) the ability of materials to absorb a broad spectrum of solar radiation, and (2) the efficient thermal management mechanisms employed during the photothermal conversion process. On the other hand, transport behavior refers to the dynamic interaction between water molecules and the material interfaces, which governs the diffusion and movement of water within the system. This phase plays a critical role in the separation of contaminants from freshwater, facilitating the effective purification process. The interplay between material properties and transport dynamics is essential for optimizing the overall performance of the evaporation system.

View Article Online
DOI: 10.1039/D5NR01104C

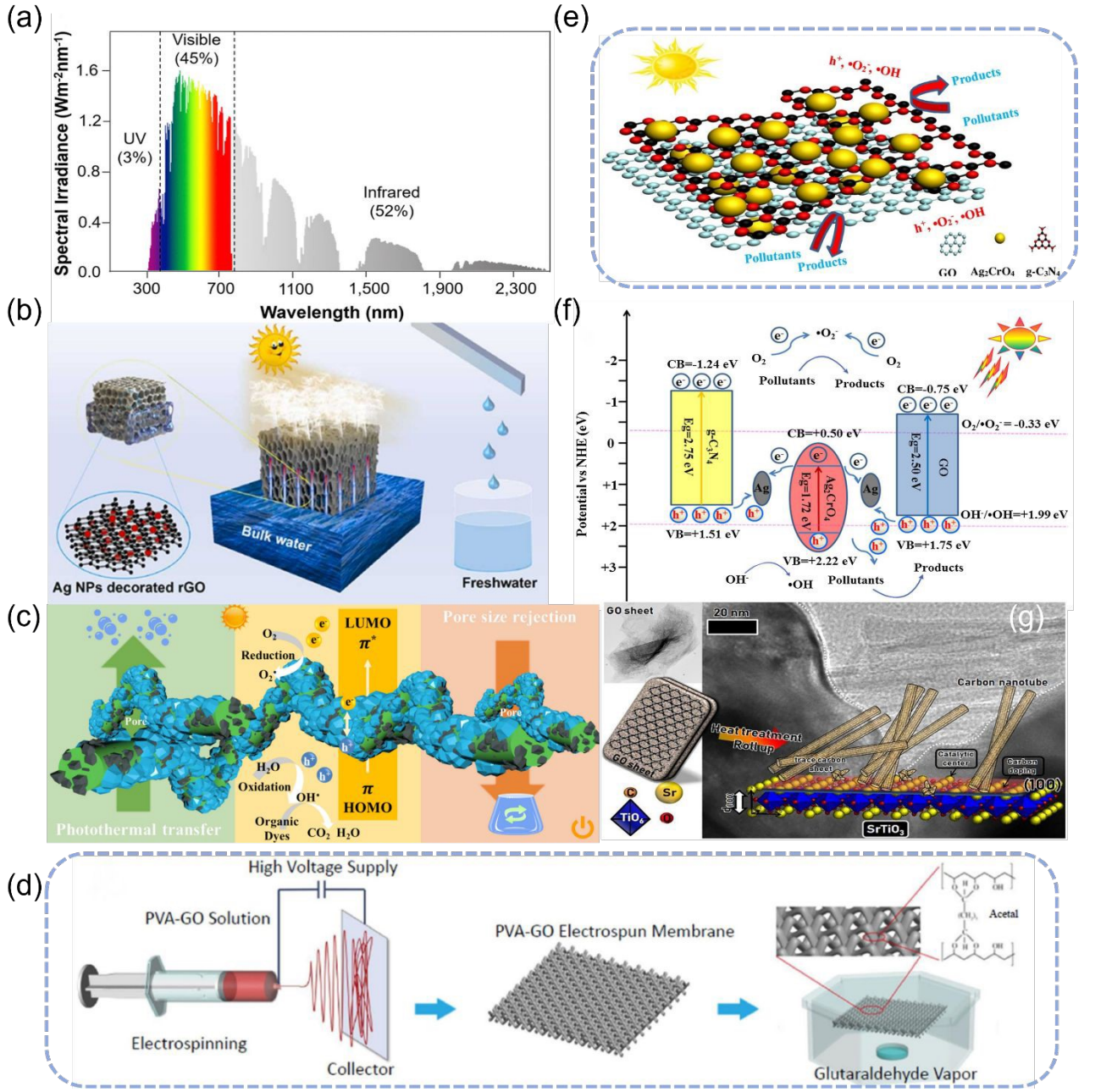

Figure 4. Strategies for enhanced solar absorption. (a) Solar spectrum. (b) rGO@Ag dual photothermal conversion material. (c) GO/PANI coupled photothermal and photocatalytic effects. (d) GO-enhanced light absorption in NPM. (e) Ternary composite photocatalyst of g-C_3N_4, GO, Ag_2CrO_4. (f) Synergy of light-induced electron-hole pair separation, multi-level charge transfer, and enhanced visible light absorption. (g) GO doping enhances light absorption in $SrTiO_3$.

We systematically examine three fundamental dimensions crucial to the design and optimization of photothermal evaporation systems: (1) the engineering of materials to enhance light absorption and thermal conversion efficiency, (2) the integration of advanced thermal management strategies to minimize heat losses and optimize temperature distribution, and (3) the refinement of transport properties to ensure efficient water vapor transport and contaminant removal. These three dimensions form the cornerstone of any successful photothermal evaporation system and will be explored in greater detail to provide comprehensive insights into the optimization strategies that can drive future advancements in this field.

3.1. Enhancement of Solar Absorption for Photothermal Conversion

Efficient solar photothermal conversion, which is critical for harnessing solar energy, depends significantly on the material's ability to capture photons across a broad spectrum and convert them into thermal energy. As depicted in Figure 4a, solar radiation spans a broad wavelength range of 250~2500 nm, including both ultraviolet (UV) and infrared (IR) wavelengths. Among these, only infrared (IR) photons directly contribute to heating the material. Therefore, it is essential for materials used in photothermal conversion to have high absorption across a broad spectral range, allowing them to effectively absorb both non-IR and IR photons and convert them into heat. The conversion process hinges on the interaction between photons and the atomic lattice, where absorbed photons excite electrons and intensify atomic vibrations, thus raising the temperature of the material. Carbon-based materials, particularly those with conjugated structures, have emerged as highly effective candidates for solar harvesting due to their ability to absorb across the full spectrum of solar radiation. These materials exhibit a unique combination of properties, including high conductivity, excellent light absorption, and strong photothermal conversion capabilities, making them ideal for improving the efficiency of solar energy capture and conversion. To further optimize solar absorption and improve photothermal performance, researchers have developed various composite strategies. One prominent approach involves the integration of GO as a key modification material. GO, known for its large surface area, high dispersibility, and tunable electronic properties, plays a crucial role in enhancing the overall performance of composite materials.

For example, Zheng et al. developed a polyvinyl alcohol (PVA) hydrogel composite that combines rGO with silver nanoparticles (AgNPs). This composite, as depicted in Figure 4b, leverages the synergy between AgNPs and rGO to prevent the aggregation of graphene layers and improve the dispersion of the nanoparticles. The result is an outstanding 97% solar absorption efficiency and less than 10% reflectance, making it an excellent candidate for photothermal conversion applications[48]. Further advancing this concept, Zhu's research team created an eco-friendly membrane made of polycaprolactone (PCL) combined with GO and polyaniline (PANI) hybrids. This hybrid structure, illustrated in Figure 4c, exhibits dual functionality, combining both photothermal and photocatalytic properties. The membrane achieves an impressive solar absorption rate of 97.44% and demonstrates a substantial evaporation rate of 1.47 $kg \cdot m^{-2} \cdot h^{-1}$ under solar irradiation of 1 $kW \cdot m^{-2}$. Additionally, it is capable of degrading 93.22% of organic dyes over a 12-hour period under the same irradiation, showcasing its potential for both energy harvesting and environmental remediation applications [49]. Moreover, Luo et al. designed a nanofiber-reinforced PVA membrane (NPM) incorporating GO and polypyrrole (PPy), as shown in Figure 4d. This composite material enhances the solar absorption capabilities of the membrane while simultaneously enabling efficient oil/water separation and desalination processes. This dual functionality makes the material highly promising for integrated applications in energy harvesting and water purification, where the efficient conversion of solar energy into heat can drive desalination processes in addition to improving energy capture [50].

Beyond photothermal applications, GO-enhanced materials have been used to design highly efficient photocatalysts. For instance, Wang et al. synthesized a ternary photocatalyst composed of g-C_3N_4, GO, and Ag_2CrO_4 through chemical precipitation. As shown in Figure 4e, the composite material exploits synergistic effects such as efficient electron-hole separation, multistage charge transfer, and enhanced visible-light absorption, significantly improving the photocatalytic degradation of organic pollutants. In particular, the composite showed superior degradation performance for compounds like rhodamine B (RhB), methylene blue (MB), phenol, and oxytetracycline, as illustrated in Figure 4f, demonstrating its potential for environmental cleanup applications [51]. In a similar vein, Hu's group developed a carbon-doped photocatalyst by incorporating GO into $SrTiO_3$, as shown in Figure 4g. This modification enhances visible light absorption, improves charge separation, and increases the density of unpaired electrons, making the photocatalyst more efficient in the degradation of azo dyes such as methyl blue and orange, as well as phenolic compounds like bisphenol A. This approach highlights the versatility of GO-based materials in enhancing both photothermal and photocatalytic functions under visible light, offering new opportunities for sustainable energy and environmental applications [52].

The integration of GO and other carbon-based materials into photothermal and photocatalytic systems offers a promising pathway to enhance solar absorption and improve energy conversion efficiency. These materials not only excel at converting solar energy into heat but also offer additional functionalities such as pollutant degradation, oil/water separation, and desalination. The continued development and optimization of these composites will likely lead to more sustainable, multifunctional materials with wide-ranging applications in renewable energy, environmental remediation, and water purification.

View Article Online
DOI: 10.1039/D5NR01104C

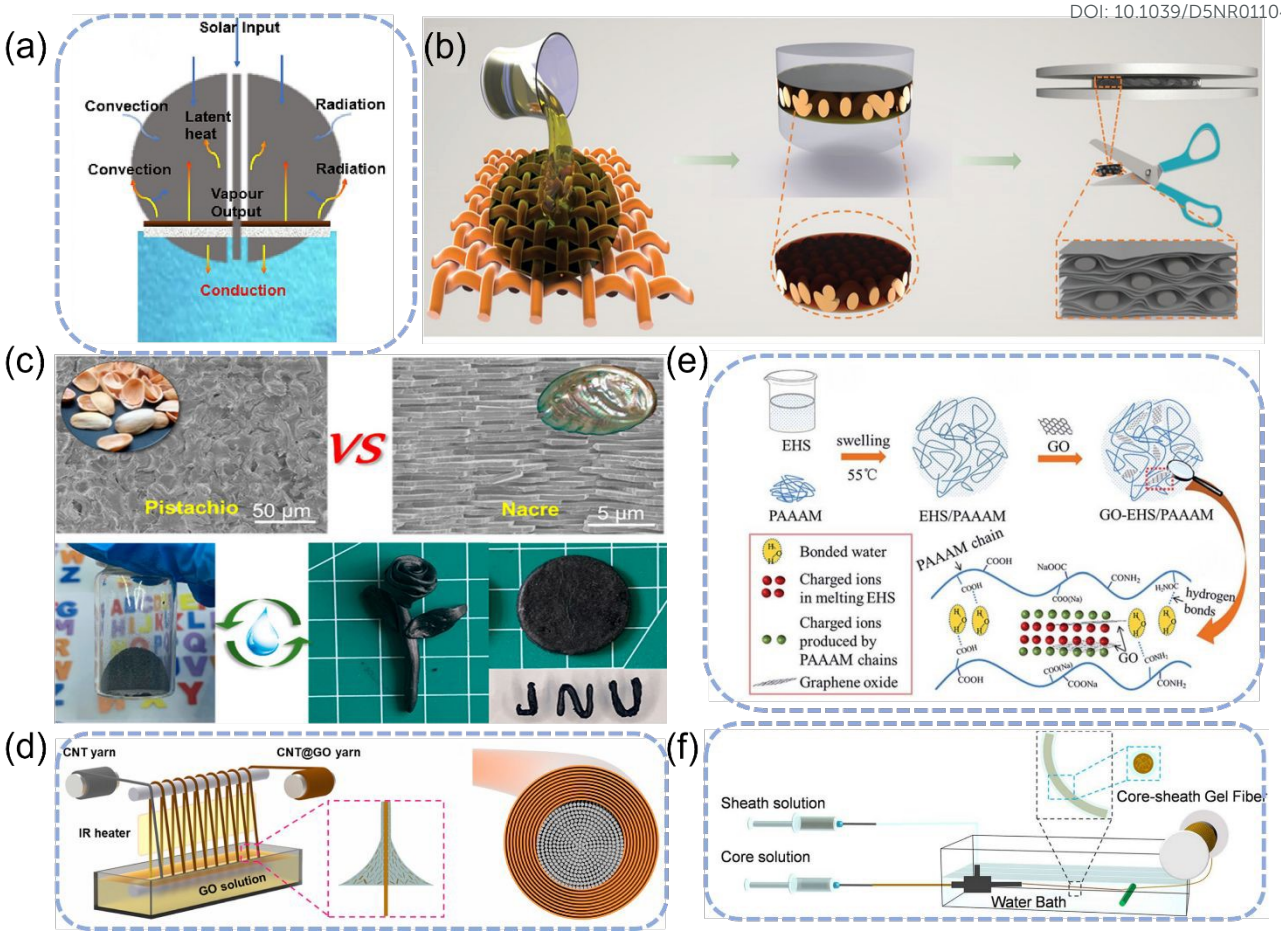

Figure 5. Thermal management optimization strategies. (a) Energy distribution in photo-thermal evaporation. (b) 3D hybrid carbon film with GO nano-wrinkles and micro-hinges. (c) GO loaded in dynamic covalent supramolecular pST system. (d) CNT@GO co-axial yarn assembly. (e) GO-EHS/PAAAM controlled phase-change synthesis. (f) Thermal-management-material-synthesis strategy for GO/SF@TPU aerogel fibers.

3.2. Advanced Thermal Management Strategies for Photothermal Conversion

In the pursuit of improving the efficiency of photothermal evaporation systems, optimizing solar absorption alongside advanced thermal management techniques represent two of the most pivotal strategies. While innovative light-harvesting designs significantly enhance spectral absorption and promote efficient photon-to-heat conversion, they serve as the foundation for maximizing energy transformation, effective thermal regulation remains equally vital to achieving high evaporation rates. Evaporation, by nature, involves a continuous energy exchange process [53] (Figure 5a), where meticulous thermal management becomes crucial in controlling temperature distribution, governing heat conduction pathways, and maintaining energy sustainability over prolonged operational periods. It is this control that ensures optimal heat transfer, limiting heat loss, reducing the risk of material degradation, and prolonging the operational life of the system. The success of this process heavily relies on the thermal conductivity properties of materials, which can be strategically enhanced by modulating hybrid orbitals in photothermal materials, creating pathways that facilitate uniform thermal distribution, and boosting evaporation efficiency.

An integral aspect of optimizing thermal management is not only focusing on the conductive properties of materials but also minimizing energy losses and material wear. A promising avenue lies in utilizing carbon-based 2D materials, which offer exceptional thermal performance and exhibit superior heat management properties. This section delves into the mechanisms by which carbon-based 2D materials, including GO and carbon nanotube (CNT)-based composites, enhance thermal conductivity and regulate phase transitions for improved thermal performance.

One remarkable development in this field is the work of Chen et al., who created a 3D hybrid carbon film by dip-coating GO onto polyimide (PI) scaffolds followed by high-temperature annealing (Figure 5b). The resulting graphitized GO/PI (g-GO/PI) film demonstrates extraordinary flexibility and anisotropic thermal conductivity, with values reaching 150 ± 7 $W \cdot m^{-1} \cdot K^{-1}$ in the through-plane direction and 1428 ± 64 $W \cdot m^{-1} \cdot K^{-1}$ in the in-plane direction. This impressive performance significantly outperforms the thermal management capacity of aluminum foil, making it an ideal candidate for high-efficiency heat

View Article Online DOI: 10.1039/D5NR01404C

transfer applications [54]. Another noteworthy advancement was made by Huang's team, who developed a pistachio-inspired nanocomposite by mechanically kneading GO into a dynamic covalent polysulfide (pST) matrix (Figure 5c). This innovative material design combines excellent recyclability, thanks to the dynamic covalent bonds in the pST matrix, with enhanced thermal conductivity (15.6 $W \cdot m^{-1} \cdot K^{-1}$), making it both sustainable and effective for heat management applications in photothermal systems [55]. In a further step toward optimizing heat transfer, Li et al. engineered aligned carbon nanotube (CNT)-GO coaxial yarns through roll-coating techniques (Figure 5d). The CNT-GO framework they developed functions as an interconnected 3D "thermal superhighway", facilitating rapid heat dissipation. The material's in-plane thermal conductivity is recorded at an impressive 804.9 $W \cdot m^{-1} \cdot K^{-1}$, while through-plane conductivity is 63.8 $W \cdot m^{-1} \cdot K^{-1}$, demonstrating its exceptional heat dissipation potential for high-efficiency photothermal evaporation [56].

In addition to enhancing conductivity, the control of phase transitions plays a crucial role in maintaining stable evaporation performance, particularly under varying thermal cycling conditions. Yang et al. developed GO-enhanced eutectic hydrated salt/poly(acrylamide-co-acrylic acid) hydrogels (GO-EHS/PAAAM) to address this challenge (Figure 5e). The incorporation of just 2 wt% GO in the composite material led to a 54% increase in thermal conductivity while maintaining chemical stability over 300 thermal cycles, demonstrating the ability to regulate phase transitions precisely and ensure the stability of evaporation systems [57]. Finally, Liu's research group introduced core-shell GO/silk fibroin (SF)@thermoplastic polyurethane (TPU) aerogel fibers, fabricated through coaxial wet-spinning techniques (Figure 5f). This innovative design was further enhanced by polyethylene glycol (PEG) impregnation, resulting in phase-change fibers (PCFs) that exhibit high latent heat storage (86.66 $J \cdot g^{-1}$) while maintaining low thermal conductivity (0.0863 $W \cdot m^{-1} \cdot K^{-1}$). These fibers not only facilitate thermal storage but also provide insulation, thus enabling the simultaneous optimization of heat storage and retention, contributing to the overall performance and longevity of the evaporation system [58].

Carbon-based 2D composites and phase-transition engineering have significantly advanced thermal management, improving photothermal evaporation efficiency. The ability to fine-tune thermal conductivity and regulate phase transitions ensures optimal performance under diverse thermal conditions, laying the groundwork for future innovations in sustainable and efficient evaporation systems.

3.3. Regulation of Water Transport Mechanisms.

The regulation of water transport mechanisms in advanced 2D materials, such as GO and graphene-like materials like GDY, plays a pivotal role in enabling efficient water purification, desalination, and proton conduction. The unique hybridization configurations of these materials not only enhance their photoresponsive properties but also offer exceptional selective interactions with water molecules and contaminants. This is achieved through meticulous electron distribution engineering and fine-tuned structural modifications that optimize their behavior in aqueous environments.

A groundbreaking study by Wang et al. demonstrated the creation of 3D GDY hollow multishell structures (HoMS) through a bottom-up synthesis approach (Figure 6a). These structures leverage sp-C orbital interactions with metal atoms, facilitating ultraselective ion removal. The resulting GDY films achieved remarkable ion concentration reductions, lowering Sr^{2+}/Cs^{+} levels by 6-7 orders of magnitude and reducing U(VI) concentrations to potable water standards. This highlights the immense potential of GDY-based materials in selective ion filtration and environmental remediation [59]. Further investigations by Meng's research group used ab initio molecular dynamics (AIMD) and density functional theory (DFT) to study GDY's proton conductivity (Figure 6b). Their findings revealed that GDY exhibits proton conductivity as high as 0.6 $S \cdot cm^{-1}$, which is four orders of magnitude higher than graphene. This exceptional conductivity is attributed to the low energy barrier (2.4 $kJ \cdot mol^{-1}$) for proton transfer across GDY's transmembrane hydrogen-bond networks, which facilitates Grotthuss-type conduction. This behavior is comparable to the proton diffusion seen in bulk water, suggesting GDY as a promising material for fuel cell applications and water splitting technologies [60]. Chen et al. demonstrated the power of hybridized materials in water purification by engineering a hierarchical evaporator that combined GO absorbers, melamine foam frameworks, and polyethyleneimine (PEI) salt-rejecting layers (Figure 6c). The synergy between GO's sp^3/sp^2 hybridization and PEI's positive charge enabled efficient electrostatic-driven desalination. This hybridized structure enhanced the material's ability to selectively reject salts while maintaining high water flux, demonstrating the importance of combining various material properties for efficient desalination processes [61]. Furthermore, Chen group developed an innovative regulatory strategy by precisely controlling the water supply rate in the rGO aerogel denoted as ICT technology, which effectively modulates the proportion of intermediate water, bound water, and free water. This approach significantly improves photothermal conversion efficiency and water evaporation rate (Figure 6d) [62].

In the realm of microstructural engineering, Lai et al. made significant strides by synthesizing centimeter-scale GDY films with ordered 1D channels on Cu(111) substrates (Figure 6e). The unique angstrom-scale, hydrophobic channels enforced a single-file water chain structure through 1D hydrogen bonding, which in turn facilitated rapid proton diffusion with diffusion coefficients as high as 1.3×10^{-4} $cm^2 \cdot s^{-1}$. This diffusion was driven by Grotthuss-type mechanisms, demonstrating the efficacy of these engineered materials in mimicking the dynamics of bulk water and paving the way for their use in proton conduction and desalination applications [63]. Zeng's group made further advances by designing submicron-thick GDY membranes on porous copper fibers (Figure 6f), which achieved a remarkable 99.9% NaCl rejection and a high flux rate of 700 $L \cdot m^{-2} \cdot h^{-1}$ in membrane distillation processes.

View Article Online
DOI: 10.1039/D5NR01104C

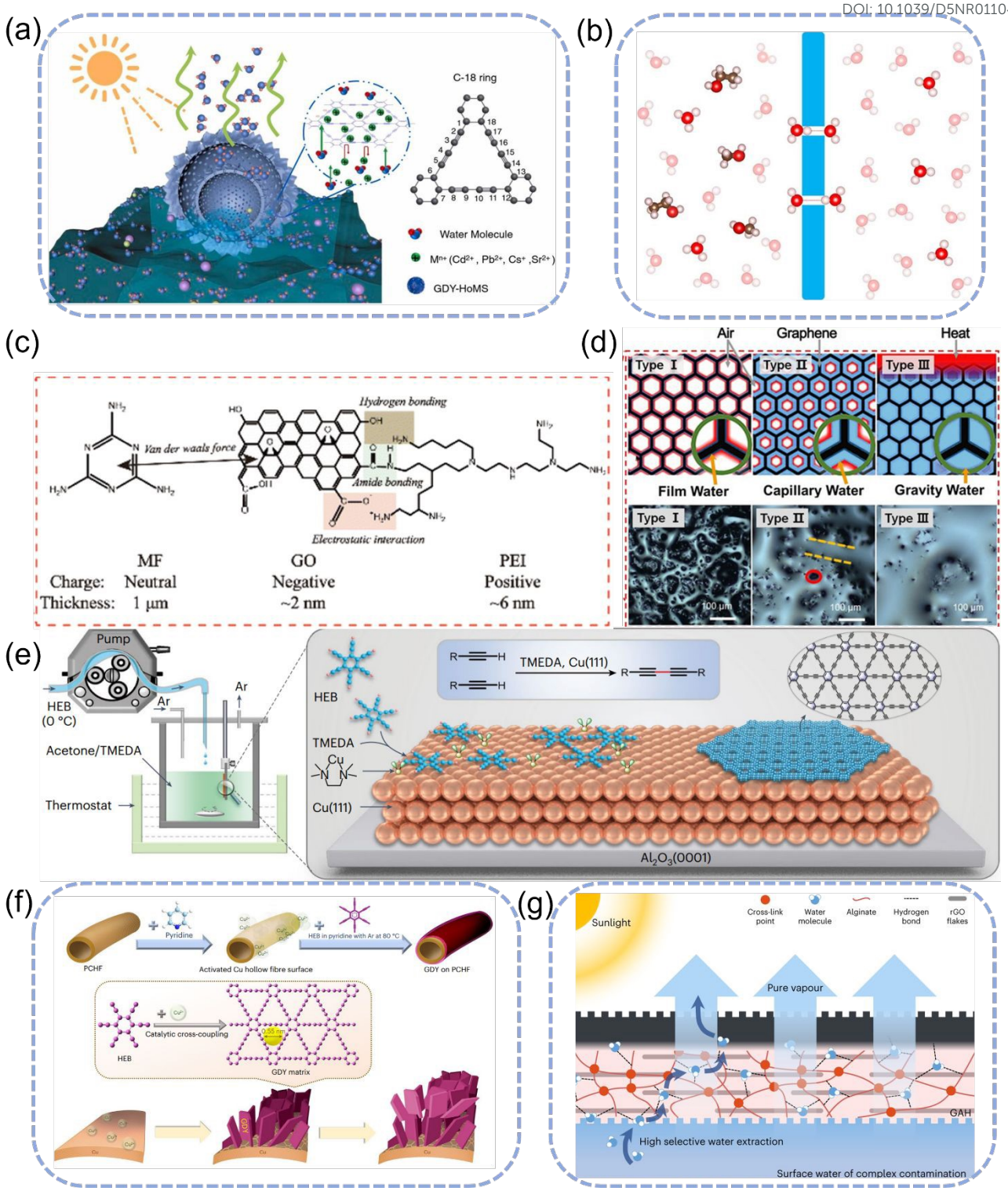

Figure 6. Strategies for regulating water transport behavior. (a) GDY intercepts heavy metal ions using its SP orbitals. (b) Theoretical verification of transmembrane hydrogen bonds in GDY membranes facilitating proton movement. (c) GO@MF@PEI hinders salt ion transport via electrostatic interaction. (d) Use injection control technology (ICT) in rGO aerogel to enhance photothermal conversion efficiency. (e) GDY crystals create 1D nanoscale water channels. (f) GO/alginate brine gel with anti-pollutant and anti-fouling ability.

These membranes outperformed traditional polymer-based membranes by 1-3 orders of magnitude, emphasizing the potential of GDY-based materials in advanced water filtration technologies [64]. Additionally, Qu group engineered a solar-

View Article Online
DOI: 10.1039/D5NR01040G

driven GO/alginate hydrogel (GAH) water extractor demonstrating exceptional anti-pollutant transport capability and superior anti-fouling performance. The GO/alginate hydrogel exhibits highly selective water transport characteristics, effectively blocking >99.5% of volatile organic compounds, >99.3% of ionic species (Na^+, Mg^{2+}, K^+, and Ca^{2+}), and 100% of non-volatile organic compounds and bacteria. Notably, the hydrogel forms an underwater contact angle exceeding 140°, creating an oil-repellent surface that achieves near-complete bacterial inactivation (≈100%) and prevents salt crystallization (Figure 6g) [65]. Furthermore, Wen's team has extensively utilized carbon-based low-dimensional materials, such as GO and CNTs [66], in the study of self-assembled ion channels. This technology not only enables the regulation of water transport behavior but also allows for the tailored control of individual ion channels [67], laying a solid foundation for advancements in the field of water evaporation.

Microstructural engineering of hybridized 2D materials such as GO and GDY, along with the development of sophisticated transport pathways, offers unparalleled control over aqueous transport processes. This emerging field holds immense promise for revolutionizing water purification, desalination, and proton conduction, addressing both environmental and energy challenges with remarkable efficiency and selectivity. The continued exploration of these advanced materials and their hybrid configurations will undoubtedly lead to new breakthroughs in sustainable water treatment and energy storage technologies.

4. Conclusion and Future Perspectives

This study provides a comprehensive analysis of 2D carbon's dual pioneers: GO and GDY, focusing on their electronic properties, microstructural characteristics, and their respective roles in enhancing the performance of photothermal evaporation systems. By considering these materials as representative examples, we break down the photothermal evaporation process into three critical aspects—solar absorption, thermal management, and water transport regulation—demonstrating how GO and GDY, through their unique structural features, can optimize system functionality. Despite the promising potential of these materials, several technical limitations persist, highlighting the need for continued research to overcome existing barriers and realize the full potential of these technologies.

For GO, a major challenge lies in its chemical reactivity and long-term stability. The oxygenated functional groups present on the carbon framework undergo spontaneous reduction upon prolonged exposure to air or immersion in water, resulting in noticeable chromatic changes (from tan to black) and the detachment of functional groups. This degradation is particularly evident during hydrothermal reduction processes used in water treatment applications, where the loss of oxygen groups leads to structural reorganization in rGO, complicating the control over its morphology and hindering reproducibility [68].

In the case of GDY, the primary limitations stem from difficulties in scaling up its synthesis. The current methods of production—chemical vapor deposition (CVD), solution-phase reactions, and solid-state synthesis—each have significant drawbacks. The CVD process allows for the preparation of large-area, uniform films with strong substrate compatibility. However, during the growth of GDY, non-uniform crystal domains often form, leading to a high defect density that can negatively impact catalytic performance [69, 70]. The solution-phase reaction method is easy to operate and well-suited for functional modifications, but controlling the reaction kinetics is challenging, and the resulting products are typically polycrystalline or amorphous [71]. The solid-state synthesis method avoids solvent contamination and is ideal for producing self-supporting films, but it suffers from uneven reaction rates and challenges in scalability [72]. Thus, there is a pressing need to develop cost-effective, scalable, and high-throughput manufacturing processes that can enhance the reproducibility and quality of GDY, making it more viable for widespread applications in catalysis, energy storage, and biomedical fields [73, 74].

The application of solar-driven evaporation technology as a potential solution to global freshwater scarcity requires overcoming several persistent challenges. Addressing these challenges calls for innovation in the design of advanced photothermal materials, specifically focused on maximizing their solar absorption and thermal efficiency while improving their structural stability. One promising approach involves orbital hybridization modulation, which enables the controlled redistribution of electrons and facilitates defect engineering and the strategic incorporation of functional groups to tailor the materials' properties. By refining the synthesis protocols for GO and GDY, it is possible to achieve precise control over their micro and nanostructural characteristics, which will better align with the evolving needs of various applications.

Furthermore, the development of application-tailored evaporators is critical for harnessing the full potential of GO and GDY in large-scale systems. Integrating the unique 2D properties of these materials into multifunctional systems could lead to significant advancements, such as the development of nanoscale water channels for selective molecular transport [65], the use of heterojunction catalysts for efficient pollutant degradation [75], and the design of thermoelectric generators that harness thermal gradients to improve energy conversion [76]. These developments would not only improve the performance of solar-driven evaporators but could also open the door to new applications in water purification, energy harvesting, and environmental remediation.

Another important aspect that must be addressed is the scaling of current photothermal evaporation systems. Presently, most evaporators are designed for small-scale applications, and their production rates are often insufficient to meet the demands of large-area applications. Future research should prioritize the development of scalable technological pathways, such as roll-to-roll deposition of GDY thin films and liquid-phase exfoliation of GO, while maintaining industrial compatibility and crystallinity. The focus should be on constructing high-throughput, large-area evaporator arrays that exhibit long-term stability under practical operating

pressures. Alternatively, derivatives of generalized carbon-based two-dimensional materials, such as COF materials, offer promising potential. Chen et al. achieved enhanced salt resistance in evaporators by utilizing Marangoni flow with COF materials [77], while Wu et al. developed an evaporator tailored for large-scale oil/water separation, leveraging the customizability of COF materials [78].

At the same time, the performance of water purification systems in practical applications must also be considered. Currently, most research focuses on laboratory-scale material design, with relatively small effective working areas (ranging from 1 cm^2 to 1 m^2). Research on the large-scale development of these devices can be broadly categorized into two approaches: one involves replicating the photothermal water purification unit [79], while the other focuses on integrating photothermal water purification materials onto large-scale commercial substrates [80, 81]. However, there remains a significant gap to bridge before the industrialization of solar-driven water purification technology, which warrants further attention.

By overcoming these challenges, it will be possible to develop more efficient and durable systems capable of addressing the growing demand for clean water in regions facing severe water scarcity.

In summary, while GO and GDY show great promise as materials for solar-driven evaporation and related applications, significant efforts are still needed to address the challenges associated with their synthesis, scalability, and integration into large-scale systems. Continued research and development in these areas will be crucial for the advancement of photothermal evaporation technologies and their eventual widespread adoption in tackling global environmental and resource challenges.

Conflicts of interest

The authors declare no interest conflict. They have no known competing financial interests or personal relationships that could have appeared to influence the work reported in this paper.

Data availability

No primary research results, software or code have been included, and no new data were generated or analysed as part of this review.

Acknowledgements

We acknowledge the financial support from the Hebei Natural Science Foundation (B2023105029), National Natural Science Foundation of China (22279010, 21671020), Natural Science Foundation of Beijing Municipality (2222075), and Analysis & Testing Center, Beijing Institute of Technology.

Notes and references

View Article Online
DOI: 10.1039/D5NR01104C

1. C. He, Z. Liu, J. Wu, X. Pan, Z. Fang, J. Li and B. A. Bryan, *Nat. Commun.*, 2021, **12**, 4667.
2. K. Elsaid, M. Kamil, T. Sayed, M. A. Abdelkareem, T. Wilberforce and A. Olabi, *Sci. Total Environ.*, 2020, **748**, 141528.
3. D. Shen, W. W. Duley, P. Peng, M. Xiao, J. Feng, L. Liu, G. Zou and Y. N. Zhou, *Adv. Mater.*, 2020, **32**, 2003722.
4. Y. Huang, C. Wang, C. Shao, B. Wang, N. Chen, H. Jin, H. Cheng and L. Qu, *Acc. Mater. Res.*, 2021, **2**, 97-107.
5. P. Zhang, H. Wang, J. Wang, Z. Ji and L. Qu, *Adv. Mater.*, 2024, **36**, 2303976.
6. P. Tao, G. Ni, C. Song, W. Shang, J. Wu, J. Zhu, G. Chen and T. Deng, *Nat. Energy*, 2018, **3**, 1031-1041.
7. C. Chen, Y. Kuang and L. Hu, *Joule*, 2019, **3**, 683-718.
8. W. Li, Z. Liang, P. Wang and Q. Ma, *Biosens. Bioelectron.*, 2024, **249**, 116008.
9. K. Yang, H. Xu, L. Cheng, C. Sun, J. Wang and Z. Liu, *Adv. Mater.*, 2012, **24**, 5586–5592.
10. Q. Zhao, J. Liu, Z. Wu, X. Xu, H. Ma, J. Hou, Q. Xu, R. Yang, K. Zhang, M. Zhang, H. Yang, W. Peng, X. Liu, C. Zhang, J. Xu and B. Lu, *Chem. Eng. J.*, 2022, **442**, 136284.
11. J. Zhou, L. Yang, X. Cao, Y. Ma, H. Sun, J. Li, Z. Zhu, R. Jiao, W. Liang and A. Li, *J. Colloid Interface Sci.*, 2024, **654**, 819-829.
12. M. Zhu, Y. Li, F. Chen, X. Zhu, J. Dai, Y. Li, Z. Yang, X. Yan, J. Song, Y. Wang, E. Hitz, W. Luo, M. Lu, B. Yang and L. Hu, *Adv. Energy Mater.*, 2017, **8**, 1701028.
13. M. S. Zielinski, J. W. Choi, T. La Grange, M. Modestino, S. M. Hashemi, Y. Pu, S. Birkhold, J. A. Hubbell and D. Psaltis, *Nano Lett.*, 2016, **16**, 2159-2167.
14. C. M. Hessel, V. P. Pattani, M. Rasch, M. G. Panthani, B. Koo, J. W. Tunnell and B. A. Korgel, *Nano Lett.*, 2011, **11**, 2560-2566.
15. D. Ding, W. Huang, C. Song, M. Yan, C. Guo and S. Liu, *Chem. Commun.*, 2017, **53**, 6744-6747.
16. X. Chen, L. Liu, P. Y. Yu and S. S. Mao, *Science*, 2011, **331**, 746-750.
17. K. K. Liu, Q. Jiang, S. Tadepalli, R. Raliya, P. Biswas, R. R. Naik and S. Singamaneni, *ACS Appl. Mater. Interfaces*, 2017, **9**, 7675-7681.
18. W. He, L. Zhou, M. Wang, Y. Cao, X. Chen and X. Hou, *Sci. Bull.*, 2021, **66**, 1472-1483.
19. E. Ye, Li, Zibiao, *Photothermal Nanomaterials*, The Royal Society of Chemistry, 2022.
20. J. Zhang, H. Chen, X. Duan, H. Sun and S. Wang, *Mater. Today*, 2023, **68**, 234-253.
21. J. D. Bernal and W. L. Bragg, *Proceedings of the Royal Society of London. Series A, Containing Papers of a Mathematical and Physical Character*, 1924, **106**, 749-773.
22. S. H. Dave, C. Gong, A. W. Robertson, J. H. Warner and J. C. Grossman, *ACS Nano*, 2016, **10**, 7515−7522.
23. X. Liu, Z. Wang, H. Liang, Y. Li, T. Liu, Q. Guo, L. Wang, Y. Yang and N. Chen, *Nanomaterials*, 2022, **12**, 1800.
24. B. Ji, N. Chen, C. Shao, Q. Liu, J. Gao, T. Xu, H. Cheng and L. Qu, *J. Mater. Chem. A*, 2019, **7**, 6766-6772.
25. L. Huang, J. Pei, H. Jiang and X. Hu, *Desalination*, 2018, **442**, 1-7.
26. X. Zhao, X. Meng, H. Zou, Z. Wang, Y. Du, Y. Shao, J. Qi and J. Qiu, *Adv. Funct. Mater.*, 2022, **33**, 2209207.
27. L. Wang, J. Lin, Y. Li, Y. Yang, X. Liu, Z. Wang, F. Liu, X. Sun, T. Yang, N. Chen and L. Qu, *J. Mater. Chem. A*, 2023, **11**, 7662-7669.

28. Y. Li, N. Chen, Z. Li, H. Shao, X. Sun, F. Liu, X. Liu, Q. Guo and L. Qu, *Adv. Mater.*, 2021, **33**, 2105853.
29. Y. Du, W. Zhou, J. Gao, X. Pan and Y. Li, *Acc. Chem. Res.*, 2020, **53**, 459-469.
30. X. Gao, H. Liu, D. Wang and J. Zhang, *Chem. Soc. Rev.*, 2019, **48**, 908-936.
31. G. Li, Y. Li, H. Liu, Y. Guo, Y. Li and D. Zhu, *Chem. Commun.*, 2010, **46**.
32. Q. Zheng, G. Luo, Q. Liu, R. Quhe, J. Zheng, K. Tang, Z. Gao, S. Nagase and J. Lu, *Nanoscale*, 2012, **4**, 3990-3996.
33. E. Sheka, *Chapter Four - Stretching and Breaking of Chemical Bonds, Correlation of Electrons, and Radical Properties of Covalent Species*, Academic Press, 2015.
34. D. Malko, C. Neiss, F. Viñes and A. Görling, *Phys. Rev. Lett.*, 2012, **108**, 086804.
35. M. S. Hybertsen and S. G. Louie, *Phys. Rev. B*, 1986, **34**, 5390-5413.
36. M. Long, L. Tang, D. Wang, Y. Li and Z. Shuai, *ACS Nano*, 2011, **5**, 2593–2600.
37. L. D. Pan, L. Z. Zhang, B. Q. Song, S. X. Du and H. J. Gao, *Appl. Phys. Lett.*, 2011, **98**, 173102.
38. B. G. Shohany, M. R. Roknabadi and A. Kompany, *Phys. E*, 2016, **84**, 146-151.
39. B. Bhattacharya, N. B. Singh and U. Sarkar, *J. Phys.:Conf. Ser.*, 2014, **566**, 012014.
40. J. Koo, M. Park, S. Hwang, B. Huang, B. Jang, Y. Kwon and H. Lee, *Phys. Chem. Chem. Phys.*, 2014, **16**, 8935-8939.
41. J. Kang, F. Wu and J. Li, *J. Phys.:Condens. Matter*, 2012, **24**, 165301.
42. R. Liu, X. Gao, J. Zhou, H. Xu, Z. Li, S. Zhang, Z. Xie, J. Zhang and Z. Liu, *Adv. Mater.*, 2017, **29**, 1604665.
43. X. Qian, H. Liu, C. Huang, S. Chen, L. Zhang, Y. Li, J. Wang and Y. Li, *Sci. Rep.*, 2015, **5**, 7756.
44. C. Yin, J. Li, T. Li, Y. Yu, Y. Kong, P. Gao, H. Peng, L. Tong and J. Zhang, *Adv. Funct. Mater.*, 2020, **30**, 2001396.
45. L. Hui, Y. Xue, H. Yu, Y. Liu, Y. Fang, C. Xing, B. Huang and Y. Li, *J. Am. Chem. Soc.*, 2019, **141**, 10677-10683.
46. Y. Du, Y. Xue, C. Zhang, Y. Liu, Y. Fang, C. Xing, F. He and Y. Li, *Adv. Energy Mater.*, 2021, **11**, 2100234.
47. X. Gao, H. Ren, J. Zhou, R. Du, C. Yin, R. Liu, H. Peng, L. Tong, Z. Liu and J. Zhang, *Chem. Mater.*, 2017, **29**, 5777-5781.
48. L. Zhu, J. Li, L. Zhong, L. Zhang, M. Zhou, H. Chen, Y. Hou and Y. Zheng, *Nano Energy*, 2022, **100**, 107441.
49. Y. Yu, Y. Yu, H. Wu, J. Shi, H. Morikawa and C. Zhu, *Adv. Fiber Mater.*, 2024, **6**, 1495-1508.
50. S. Chen, Y. Liu, Y. Wang, K. Xu, X. Zhang, W. Zhong, G. Luo and M. Xing, *Chem. Eng. J.*, 2021, **411**, 128042.
51. F. Chen, Q. Yang, S. Wang, F. Yao, J. Sun, Y. Wang, C. Zhang, X. Li, C. Niu, D. Wang and G. Zeng, *Appl. Catal., B*, 2017, **209**, 493-505.
52. C.-W. Chang and C. Hu, *Chem. Eng. J.*, 2020, **383**, 123116.
53. U. Misra, N. H. Barbhuiya, Z. H. Rather and S. P. Singh, *Adv. Colloid Interface Sci.*, 2024, **327**, 103154.
54. Y. Li, Y. Zhu, G. Jiang, Z. P. Cano, J. Yang, J. Wang, J. Liu, X. Chen and Z. Chen, *Small*, 2020, **16**, 1903315.
55. Y. Wang, Y. Zhang, Z. Zhang, T. Li, J. Jiang, X. Zhang, T. Liu, J. Qiao, J. Huang and W. Dong, *ACS nano*, 2022, **16**, 3394–3403.
56. D. Liu, Z. Yang, Y. Zhang, S. Wang, Y. Niu, J. Yang, X. Yang, H. Fu, L. Chen, Z. Yong and Q. Li, *Carbon*, 2023, **208**, 322-329.
57. Y. Liu, Y. Yang and S. Li, *J. Mater. Chem. A*, 2016, **4**, 18134-18143.
58. W. Xu, C. Ren, Z. Wang, B. Lochab, J. Liu, Y. Zhang and L. Wu, *J. Mater. Chem. A*, 2025, **17**, 7081-7090.
59. S. Zhan, X. Chen, B. Xu, L. Wang, L. Tong, R. Yu, N. Yang and D. Wang, *Nano Today*, 2022, **47**, 101626.
60. J. Xu, H. Jiang, Y. Shen, X.-Z. Li, E. G. Wang and S. Meng, *Nat. Commun.*, 2019, **10**, 3971.
61. Z. Yang, L. Chen, K. Yang, C. Chen, Y. Zhang, S. Li, C. Chu, X. Zhu and B. Chen, *J. Mater. Chem. A*, 2022, **10**, 24373-24380.
62. H. Liang, Q. Liao, N. Chen, Y. Liang, G. Lv, P. Zhang, B. Lu and L. Qu, *Angew. Chem., Int. Ed.* , 2019, **58**, 19041-19046.
63. J. Li, K. Zhou, Q. Liu, B. Tian, X. Liu, L. Cao, H. Cao, G. Li, X. Zhang, Y. Han and Z. Lai, *Nat. Water*, 2025, DOI: 10.1038/s44221-025-00397-9.
64. H. Chen, X. Liu, D. Gong, C. Zhu, G. Liu, J. Fan, P. Wu, Z. Li, Y. Pan, G. Shi, Y. Sun and G. Zeng, *Nat. Water*, 2023, **1**, 800-807.
65. X. Hao, H. Yao, P. Zhang, Q. Liao, K. Zhu, J. Chang, H. Cheng, J. Yuan and L. Qu, *Nat. Water*, 2023, **1**, 982-991.
66. W. Xin, L. Jiang and L. Wen, *Angew. Chem., Int. Ed.*, 2022, **61**, e202207369.
67. Y. Hu, H. Xiao, L. Fu, P. Liu, Y. Wu, W. Chen, Y. Qian, S. Zhou, X. y. Kong, Z. Zhang, L. Jiang and L. Wen, *Adv. Mater.*, 2023, **35**, 2301285.
68. S. Zhou, K. Guan, Z. Li, P. Xu, S. Fang, A. Zhang, Z. Wang, S. He, K. Nakagawa and H. Matsuyama, *Small*, 2024, **20**, 2311237.
69. Y. Gao, Y. Xue, S. Chen, Y. Zheng, S. Chen, X. Zheng, F. He, C. Huang and Y. Li, *Angew. Chem., Int. Ed.*, 2024, **63**, e202406043.
70. Z. Zhang, X. Feng, Z. Zhang, L. Chen, W. Liu, L. Tong, X. Gao and J. Zhang, *J. Am. Chem. Soc.*, 2024, **146**, 14898-14904.
71. L. Gao, S. Wang, F. Wang, Z. Yang, X. Li, J. Gao, D. Fazzi, X. Ye, X. Wang and C. Huang, *ACS Nano*, 2024, **18**, 30368-30377.
72. K. Ma, J. Wu, X. Wang, Y. Sun, Z. Xiong, F. Dai, H. Bai, Y. Xie, Z. Kang and Y. Zhang, *Angew. Chem., Int. Ed.*, 2022, **61**, e202211094.
73. C. Chang, H. Lu, Y. Liu, G. Long, X. Guo, X. Ji and Z. Jin, *J. Mater. Chem. A*, 2024, **12**, 4204-4220.
74. Z. Jia, Y. Li, Z. Zuo, H. Liu, C. Huang and Y. Li, *Acc. Chem. Res.*, 2017, **50**, 2470-2478.
75 X. He, Z. Wang, Z. Geng, J. Liu, Z. Jin and N. Chen, *Adv. Funct. Mater.*, 2025, 2505818.
76. R. Niu, J. Ren, J. J. Koh, L. Chen, J. Gong, J. Qu, X. Xu, J. Azadmanjiri and J. Min, *Adv. Energy Mater.*, 2023, **13**, 2302451.
77. X. Yu, M. Xia, Y. Zhao, Q. Bao, W. Wang, Y. Li, Z. Sui, J. Xiao and Q. Chen, *Chem. Eng. J.*, 2024, **501**, 157500.
78. F. Wang, Y. Wang, Y. Zhang, H. Wang and D. Wu, *Small*, 2025, **21**, 2409382.
79. C. Chen, L. Zhou, J. Yu, Y. Wang, S. Nie, S. Zhu and J. Zhu, *Nano Energy*, 2018, **51**, 451-456.
80. S. Zhang, H. Ma, D. Guo, P. Guo, J. Wang, M. Liu, S. Wu and C. Bao, *ACS Appl. Nano Mater.*, 2022, **5**, 7198-7207.
81. L. Cui, P. Zhang, Y. Xiao, Y. Liang, H. Liang, Z. Cheng and L. Qu, *Adv. Mater.*, 2018, **30**, 1706805.

View Article Online
DOI: 10.1039/D5NR01104C

Data Availability Statement

Data sharing is not applicable to this article as no new data were created or analyzed in this study.